

Multiwalled nanotube faceting unravelled

Itai Leven, Roberto Guerra, Andrea Vanossi, Erio Tosatti, and Oded Hod

1. Achiral DWCNTs optimized using the Tersoff intra-layer potential

In the main text we have presented optimized structures of various DWCNTs obtained using the Airebo¹ intra-layer and Kolmogorov-Crespi² interlayer force fields. Here, in order to verify the robustness of our results against the choice of intra-layer force-field we have repeated the calculations using the Tersoff³ intra-layer potential. Comparing the optimized AC@AC systems presented in Fig. 1 of the main text and those shown in Fig. S1 we find that the relaxed structures present very similar faceting behavior for both intra-layer potentials. The ZZ@ZZ DWCNTs exhibit less faceting when optimized using the Tersoff potential than with the Airebo force-field. Furthermore, using the former, the widest DWCNT considered (20 nm in diameter) already exhibits a circular cross section thus indicating the existence of a maximal critical faceting diameter. Nevertheless, the qualitative behavior that originates from the basic symmetries of the system remains valid for both force-fields.

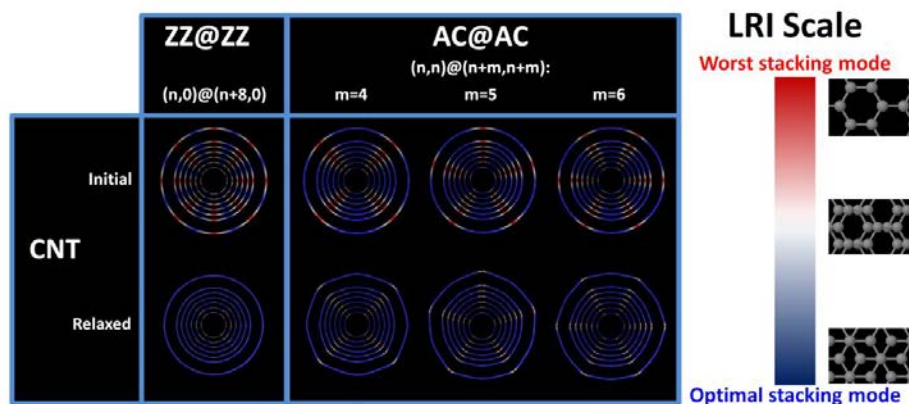


Figure S1: Relaxed achiral DWCNTs geometries and LRI patterns obtained using the Tersoff intralayer and the Kolmogorov-Crespi interlayer potentials. Schematic representation of achiral DWCNTs showing their structure and local registry patterns before (upper row) and after (lower row) geometry relaxation. Each frame includes seven DWNTs with diameters in the range of 5-20 nm. Four groups of DWNTs are presented (from left to right): ZZ@ZZ $(n,0)@(n+8,0)$; AC@AC $(n,n)@(n+4,n+4)$, $(n,n)@(n+5,n+5)$, and $(n,n)@(n+6,n+6)$. For the ZZ@ZZ systems we choose $n=55, 80, 105, 130, 155, 180,$ and 243 ; For the AC@AC systems we use $n=31, 46, 60, 75, 89, 104,$ and 140 . The LRI color bar is shown on the right.

2. AC@ZZ DWCNTs

In Fig. 1 of the main text we have presented optimized structures of achiral DWCNTs. In the case of the mixed achiral ZZ@AC systems it was shown that the interlayer registry patterns are homogeneous and hence no faceting occurs. For completeness we have repeated these calculations on the (144,144)@(258,0) AC@ZZ DWCNT. Here, as well, a similar behavior was observed thus verifying that the mixed achiral nanotubes are not expected to exhibit facets.

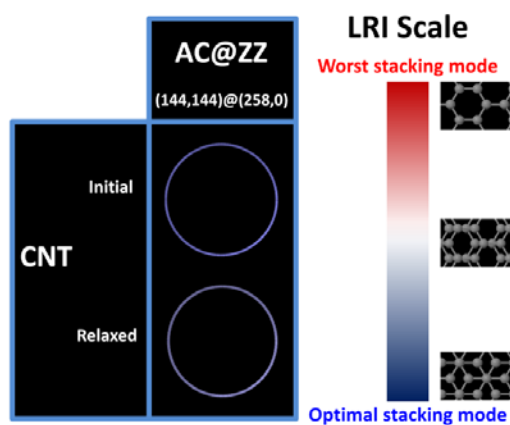


Figure S2: Structure and LRI patterns of an AC@ZZ DWCNT. Schematic representation of the (144,144)@(258,0) DWCNT before (upper panel) and after (lower panel) geometry optimization using the Airebo intralayer and Kolmogorov-Crespi interlayer potentials. The LRI color bar is shown on the right.

3. Chiral DWCNTs optimized using the Aierbo intra-layer potential

In Fig. 2 of the main text we presented optimized structures of chiral DWBNNTs obtained using the Tersoff interlayer potential and the *h*-BN ILP.⁴ For completeness, we present in Fig. S3 the corresponding relaxed chiral DWCNT structures obtained using the Airebo intralayer and Kolmogorov-Crespi interlayer potentials. Notably, despite the different nature of the intralayer covalent bonding of the two systems very similar faceting patterns appears for DWBNNTs and DWCNTs of the same identity. This further supports our conclusion that the origin of faceting is geometric.

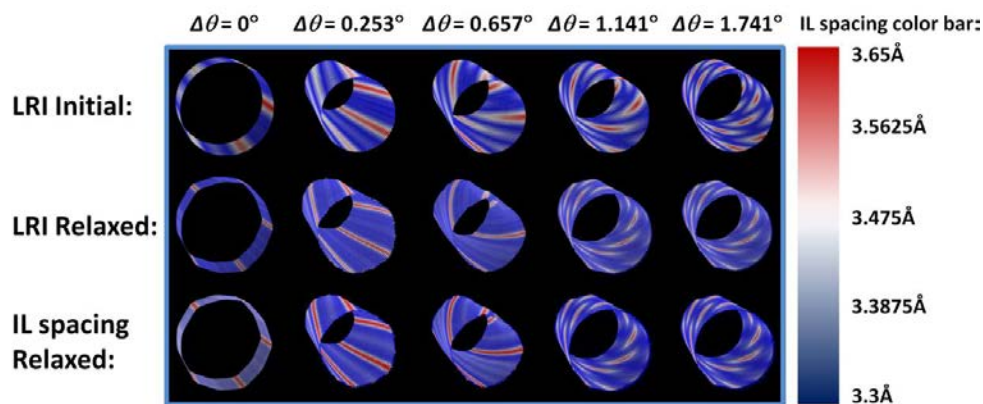


Figure S3: Relaxed chiral DWCNTs geometries, LRI patterns, and interlayer distances obtained using the Airebo Intralayer and Kolmogorov-Crespi interlayer potentials. Schematic representation of (120,100)@(126,105) (leftmost column), (60,60)@(66,65) (second column), (70,70)@(77,74) (third column), (68,68)@(75,70) (fourth column), and (71,71)@(80,72) (rightmost column) DWCNTs showing their local registry patterns before (upper row) and after (middle row) geometry relaxation. The lower row presents the interlayer spacing with the corresponding color bar appearing on the right (note that the colorbar scale here differs from that appearing in the main text for DWBNNTs). The LRI color bar is the same as in Fig. S1 of the main text. The chiral angle difference between the inner and outer shells, $\Delta\theta$, is indicated above the respective columns.

4. The local registry index (LRI)

The local registry index is a tool developed to quantify the degree of local inter-surface registry matching at rigid material interfaces. The LRI is derived from the global registry index (GRI) concept that provides a quantitative measure of the overall interfacial registry matching.⁵ In the LRI scheme each atom is assigned a number between 0 (for optimal local stacking) and 1 (for worst local stacking) that characterizes the favorability of its local stacking configuration. To this end, each atomic position is given a circle (or, alternatively, a two-dimensional Gaussian function) lying in its respective surface plane. The projected overlaps of pairs of atomic circles (or Gaussians) lying in adjacent layers are then used to construct the registry index. In the original implementation of the registry index method for flat parallel surfaces, the pair circle overlaps were calculated using a simple analytic formula as a function of the lateral distance $\rho_{in} = \rho_{ni}$ between each atomic pair (i and n) in adjacent layers. Here, the lateral distance was defined as the distance between atom n of one layer and the surface normal at the position of atom i of the other layer. The latter was taken as the normal to the surface defined by the three nearest-neighbors of atom i within the hexagonal lattice (see Fig. S4). Adopting this definition for the case of curved surfaces lifts the symmetry of the lateral distance such that $\rho_{in} \neq \rho_{ni}$. To account for this, the circle pair overlap is taken as the mean overlap calculated using ρ_{in} and ρ_{ni} in the following manner

$$S_{in} = 0.5 \cdot [S(\rho_{in}) + S(\rho_{ni})],$$

where $S(\rho_{in})$ and $S(\rho_{ni})$ are the circle overlaps of atoms i and n calculated at lateral distances ρ_{in} and ρ_{ni} , respectively, and S_{in} is the mean overlap area of the atomic pair. With this definition the pair overlap becomes dependent on the relative spatial orientation of the two circles and reduces with increasing inter-circle tilt angle.

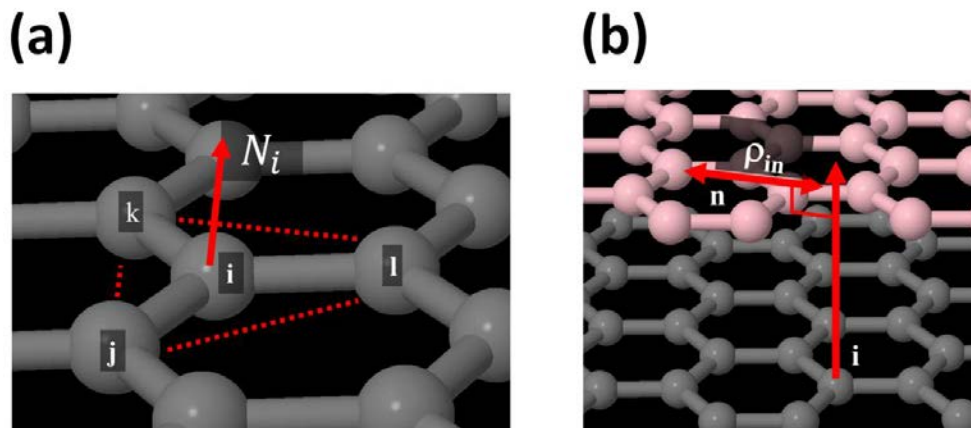


Figure S4: Normal and lateral distance definitions. (a) The surface normal at the position of atom i , N_i , is defined as the normal to the plane formed by its three nearest-neighbors j , k and l . (b) The lateral distance ρ_{in} is taken as the shortest distance between atom n of one layer and the normal associated with atom i of the other layer. For the sake of simplicity and clarity we show here a bilayer graphene system and color the upper layer atoms in pink. The same definition holds for h -BN based systems.

The local registry index of atom i is simply defined as the average global RI of this atom and its three nearest neighbors with the entire adjacent layer. As an example, for graphitic systems one needs to sum the pair overlaps of carbon atom i with all atomic carbon centers of the adjacent layer, S_i^{CC} . Similarly, the corresponding pair overlaps of its three nearest neighboring atoms j , k , and, l with all atoms of the adjacent layer S_j^{CC} , S_k^{CC} , and S_l^{CC} are evaluated. With this, the local registry index of atom i is defined as:

$$LRI_i^{graphene} = \frac{1}{3} \sum_{n=j,k,l} \frac{(S_i^{CC} + S_n^{CC}) - (S_i^{CC,Opt} + S_n^{CC,Opt})}{(S_i^{CC,Worst} + S_n^{CC,Worst}) - (S_i^{CC,Opt} + S_n^{CC,Opt})}$$

where we have averaged over the contributions of all nearest neighboring atoms j , k , and l of atom i . Here, $S_m^{CC,Opt}$ and $S_m^{CC,Worst}$ are the sum of pair overlaps of the circle associated with atom m on one layer and all circles of the adjacent layer obtained at the optimal and worst local stacking modes, respectively (see Fig. S5). This definition yields a value of 0 for the optimal local stacking mode and 1 for the worst local stacking mode.

Similarly, the normalized local registry index for h -BN is given by

$$LRI_{h-BN} = \frac{1}{3} \sum_{n=j,k,l} \frac{[(S_i^{NN} + S_n^{NN}) - (S_i^{NN,Opt} + S_n^{NN,Opt})] + [(S_i^{BB} + S_n^{BB}) - (S_i^{BB,Opt} + S_n^{BB,Opt})] - [(S_i^{NB} + S_n^{NB}) - (S_i^{NB,Opt} + S_n^{NB,Opt})]}{[(S_i^{NN,Worst} + S_n^{NN,Worst}) - (S_i^{NN,Opt} + S_n^{NN,Opt})] + [(S_i^{BB,Worst} + S_n^{BB,Worst}) - (S_i^{BB,Opt} + S_n^{BB,Opt})] - [(S_i^{NB,Worst} + S_n^{NB,Worst}) - (S_i^{NB,Opt} + S_n^{NB,Opt})]}$$

where $S_m^{MN,Opt}$ and $S_m^{MN,Worst}$ are the sum of pair overlaps of the circle associated with atom m of type M on one layer and all circles of type N on the adjacent layer obtained at the optimal and worst local stacking modes, respectively.

In the present calculations, we adopt the circle radii of the GRI method where $r_C = 0.5a_{CC}$, $r_B = 0.15a_{BN}$, and $r_N = 0.5a_{BN}$, and $a_{CC} = 1.42 \text{ \AA}$ and $a_{BN} = 1.446 \text{ \AA}$ are the CC and BN intralayer covalent bond lengths, respectively.

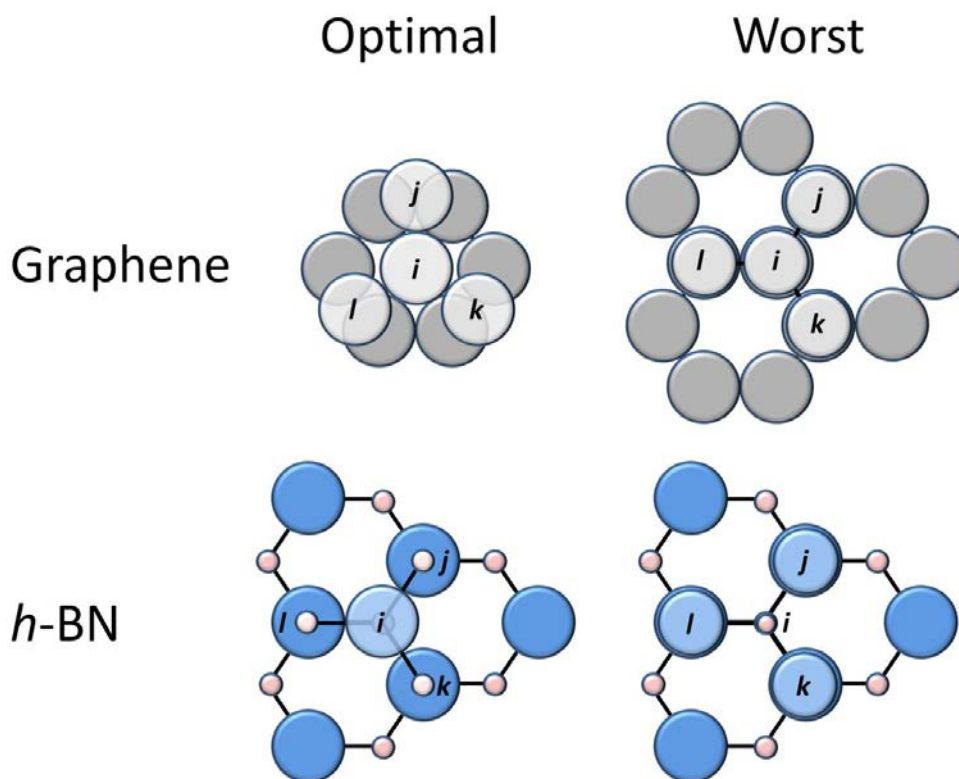


Figure S5: LRI optimal and worst stacking configurations. Schematic representation of the optimal (left) and worst (right) local stacking configurations of atom i and its three nearest neighbors j , k and l in bilayer graphene (top) and h -BN (bottom). Note that in the LRI definition of graphene the optimal configuration differs from the global minimum energy AB stacking mode. Pink and Blue circles represent boron and nitrogen atoms, respectively.

5. Frozen partial charges approximation in the *h*-BN ILP calculations

For the geometry optimizations of the BNNTs we used our recently developed interlayer potential (ILP) for *h*-BN.⁴ In our original implementation of the *h*-BN ILP one of the most computationally intensive steps was the partial atomic charge calculation performed using the electronegativity equalization method (EEM). In order to reduce the computational burden in the present calculations we adopted the frozen charge approximation assuming constant partial charges of +0.47e and -0.47e for the boron and nitrogen atoms, respectively. This approximation was found to lower the interlayer sliding energy landscape corrugation and therefore the *h*-BN ILP was reparameterized to reproduce the TS-vdW corrected PBE sliding landscapes of bi-layer *h*-BN reported in Ref. 6. To this end, the repulsive *NN* parameters β_{ij} and γ_{ij} , representing the range of the repulsion term and the width of the Gaussian decay in the anisotropic term (see Ref. 4), were modified from 3.69 Å and 1.2 Å to 3.8 Å and 0.8 Å, respectively. The above reparameterization yields a sliding corrugation of 6.54 meV/atom (see Fig. S6) and a binding energy of 35.1 meV/atom (see Fig. S7), which are in good agreement with the reference values of 6.5 meV/atom and 38.1 meV/atom, respectively, obtained using the TS-vdW dispersion corrected DFT approach.⁶

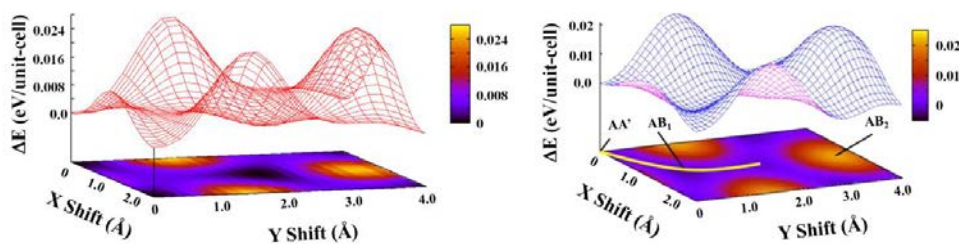


Figure S6: Left: Sliding energy landscape of a periodic bi-layer *h*-BN system calculated within the frozen partial charge approximation using the *h*-BN ILP with the parameterization presented herein. For comparison purposes the reference sliding energy landscape calculated using the TS-vdW dispersion corrected PBE density functional approximation with the tier-2 basis set within the FHI-AIMS code is presented on the right.⁶

6. Many body dispersion effects

The parameterization of the interlayer force-field terms used in the present study does not take into account many-body dispersion (MBD) effects. Recent results obtained via state of the art PBE exchange-correlation density functional calculations augmented by a MBD treatment of long-range correlation reported a binding energy of 25 meV/atom for bi-layer *h*-BN.⁷ As may be expected, this value is considerably lower than the original *h*-BN ILP binding energy of 35.1 meV/atom, neglecting MBD effects. To verify that our predictions are robust against the inclusion of such screening effects we have repeated our calculations for six of the achiral DWBNNTs studied in the main text while artificially reducing the interlayer binding energy to match the screened value. To this end, we have reduced all C_6 coefficients by 17%. The resulting binding energy curves appear in Fig. S7.

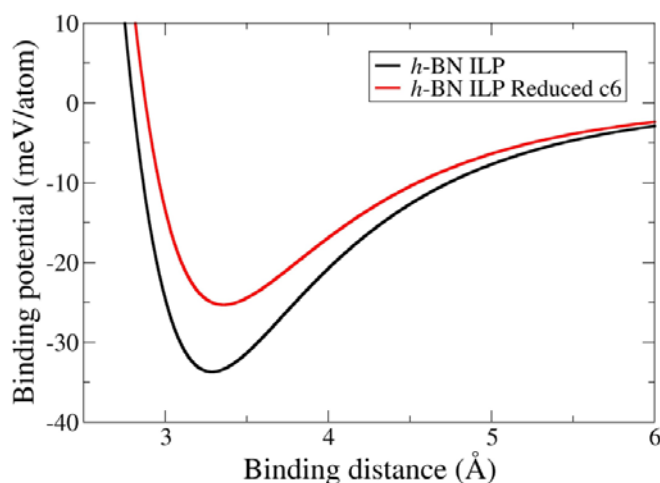


Figure S7: Binding energy curves of periodic bi-layer *h*-BN calculated with the original *h*-BN ILP parameterization (full black line) and after C_6 coefficients reduction by 17% (full red line).

The resulting relaxed structures that are shown in Fig. S8 demonstrate clear faceting of similar nature to those presented in the main text even with the reduced binding energy thus indicating the generality of our findings. More research on incorporating MBD effects in dedicated interlayer potentials is currently being pursued.

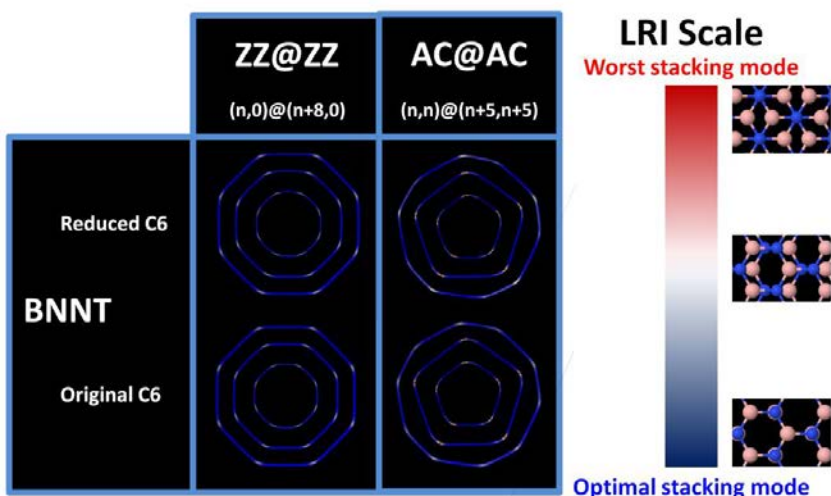


Figure S8: Relaxed achiral DWBNNTs geometries and LRI patterns obtained using the *h*-BN ILP potential with reduced C_6 coefficients (upper panels). Each frame includes 3 DWNTs with diameters in the range of 9-20 nm. Two groups of DWNTs are presented: ZZ@ZZ $(n,0)@(n+8,0)$ (left) and AC@AC $(n,n)@(n+5,n+5)$ (right). For the ZZ@ZZ systems we choose $n=105, 180,$ and 243 ; For the AC@AC systems we use $n=60, 104,$ and 140 . For comparison purposes the corresponding relaxed structures appearing the main text obtained using the original *h*-BN ILP parameterization are presented in the lower panels.

7. Moiré superlattice unit cell characterization via 2D mapping

Consider the $(n, m)@(n', m')$ double walled nanotube having chiral vectors of $\mathbf{c}_h = n\mathbf{a}_1 + m\mathbf{a}_2$ and $\mathbf{c}'_h = n'\mathbf{a}_1 + m'\mathbf{a}_2$ for the inner and outer shells, respectively. Here, $\mathbf{a}_1 = \left(\frac{3}{2}, \frac{\sqrt{3}}{2}\right)d$ and $\mathbf{a}_2 = \left(\frac{3}{2}, -\frac{\sqrt{3}}{2}\right)d$ are the primitive unit-cell vectors of the hexagonal lattice written in the (x, y) coordinate system with the x axis pointing along the armchair direction and the y axis along the perpendicular zigzag axis and d is the inter-site distance (see Fig. S9). In order to explain the interlayer registry patterns discussed in the main text the two tubes are first unrolled to obtain infinite ribbons of width $c_h = |\mathbf{c}_h|$ (see shaded green area) and $c'_h = |\mathbf{c}'_h|$ (see shaded blue area) representing the inner and outer walls, respectively. Next, the ribbon representing the outer wall is rotated by an angle $\Delta\theta = \theta' - \theta$, where $\theta = \arctg\left(\frac{\sqrt{3}m}{m+2n}\right)$ and $\theta' = \arctg\left(\frac{\sqrt{3}m'}{m'+2n'}\right)$ are the chiral angles of the inner and outer shells, respectively, such that the chiral vectors of the two walls point in the same direction using the following rotation matrix:

$$\mathcal{R} = \begin{pmatrix} \cos(\Delta\theta) & -\sin(\Delta\theta) \\ \sin(\Delta\theta) & \cos(\Delta\theta) \end{pmatrix}.$$

Finally, in order to mimic the curvature difference between the two tube layers the outer shell is now contracted along its finite dimension until the chiral vectors of the two ribbons fully overlap using the following operation.^{5,8,9}

$$\mathcal{M} = \begin{pmatrix} c_h/c'_h & 0 \\ 0 & 1 \end{pmatrix}.$$

This assures that radially aligned atoms in the cylindrical configuration are also eclipsed in the planar representation. Note that this matrix is written in the rotated coordinate system (\hat{x}, \hat{y}) whose x -axis is parallel to \mathbf{c}_h . The corresponding transformation between the original and rotated coordinate systems is given by:

$$\begin{cases} \hat{x} = \cos\left(\theta - \frac{\pi}{6}\right)\hat{x} - \sin\left(\theta - \frac{\pi}{6}\right)\hat{y} \\ \hat{y} = \sin\left(\theta - \frac{\pi}{6}\right)\hat{x} + \cos\left(\theta - \frac{\pi}{6}\right)\hat{y} \end{cases}$$

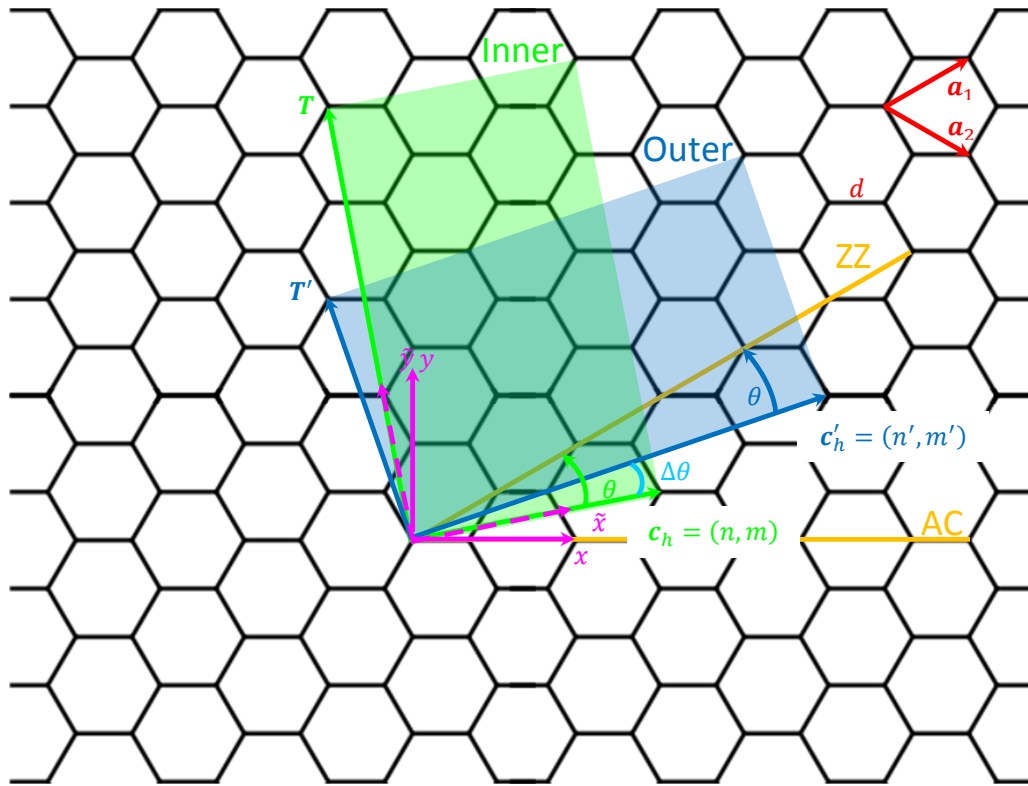


Figure S9: Planar representation of unrolled double walled nanotubes.

The lattice vectors of the resulting Moiré supercell are given by:⁸

$$\mathbf{L}_i^M = (I - \mathcal{R}^{-1}\mathcal{M}^{-1})^{-1}\tilde{\mathbf{a}}_i$$

where I is the 2x2 unit matrix and $\tilde{\mathbf{a}}_i$ are the primitive graphene lattice vectors written in the rotated coordinate system (\tilde{x}, \tilde{y}) as $\tilde{\mathbf{a}}_1 = \sqrt{3}d(\cos(\theta), \sin(\theta))$ and $\tilde{\mathbf{a}}_2 = \sqrt{3}d(\cos(\theta - \frac{\pi}{3}), \sin(\theta - \frac{\pi}{3}))$. The inverse matrix of the rotation matrix is a rotation in the opposite direction given by:

$$\hat{\mathcal{R}}^{-1} = \begin{pmatrix} \cos(\Delta\theta) & \sin(\Delta\theta) \\ -\sin(\Delta\theta) & \cos(\Delta\theta) \end{pmatrix},$$

And the inverse of the contraction matrix is the corresponding expansion matrix:

$$\hat{\mathcal{M}}^{-1} = \begin{pmatrix} c'_h/c_h & 0 \\ 0 & 1 \end{pmatrix}.$$

With this we may write:

$$\begin{aligned}\hat{I} - \mathcal{R}^{-1}\mathcal{M}^{-1} &= \begin{pmatrix} 1 & 0 \\ 0 & 1 \end{pmatrix} - \begin{pmatrix} \cos(\Delta\theta) & \sin(\Delta\theta) \\ -\sin(\Delta\theta) & \cos(\Delta\theta) \end{pmatrix} \begin{pmatrix} c'_h/c_h & 0 \\ 0 & 1 \end{pmatrix} \\ &= \begin{pmatrix} 1 & 0 \\ 0 & 1 \end{pmatrix} - \begin{pmatrix} (c'_h/c_h)\cos(\Delta\theta) & \sin(\Delta\theta) \\ -(c'_h/c_h)\sin(\Delta\theta) & \cos(\Delta\theta) \end{pmatrix} \\ &= \begin{pmatrix} 1 - (c'_h/c_h)\cos(\Delta\theta) & -\sin(\Delta\theta) \\ (c'_h/c_h)\sin(\Delta\theta) & 1 - \cos(\Delta\theta) \end{pmatrix}.\end{aligned}$$

Inverting this we obtain:

$$\begin{aligned}(\hat{I} - \hat{R}^{-1}\hat{M}^{-1})^{-1} &= \frac{1}{[1 - (c'_h/c_h)\cos(\Delta\theta)][1 - \cos(\Delta\theta)] + (c'_h/c_h)\sin^2(\Delta\theta)} \begin{pmatrix} 1 - \cos(\Delta\theta) & \sin(\Delta\theta) \\ -(c'_h/c_h)\sin(\Delta\theta) & 1 - (c'_h/c_h)\cos(\Delta\theta) \end{pmatrix} \\ &= \frac{1}{(1 + c'_h/c_h)[1 - \cos(\Delta\theta)]} \begin{pmatrix} 1 - \cos(\Delta\theta) & \sin(\Delta\theta) \\ -(c'_h/c_h)\sin(\Delta\theta) & 1 - (c'_h/c_h)\cos(\Delta\theta) \end{pmatrix}\end{aligned}$$

The first Moiré supercell lattice vector L_1^M

The first Moiré supercell lattice vector is given by:

$$\begin{aligned}L_1^M &= (I - \mathcal{R}^{-1}\mathcal{M}^{-1})^{-1}\tilde{\alpha}_1 \\ &= \frac{\sqrt{3}d}{(1 + c'_h/c_h)[1 - \cos(\Delta\theta)]} \begin{pmatrix} 1 - \cos(\Delta\theta) & \sin(\Delta\theta) \\ -(c'_h/c_h)\sin(\Delta\theta) & 1 - (c'_h/c_h)\cos(\Delta\theta) \end{pmatrix} \begin{pmatrix} \cos(\theta) \\ \sin(\theta) \end{pmatrix} \\ &= \frac{\sqrt{3}d}{(1 + c'_h/c_h)[1 - \cos(\Delta\theta)]} \begin{pmatrix} [1 - \cos(\Delta\theta)]\cos(\theta) + \sin(\Delta\theta)\sin(\theta) \\ -(c'_h/c_h)\sin(\Delta\theta)\cos(\theta) + [1 - (c'_h/c_h)\cos(\Delta\theta)]\sin(\theta) \end{pmatrix}\end{aligned}$$

Looking separately on each vector element we get:

$$\begin{aligned}[1 - \cos(\Delta\theta)]\cos(\theta) + \sin(\Delta\theta)\sin(\theta) &= \cos(\theta) - [\cos(\Delta\theta)\cos(\theta) - \sin(\Delta\theta)\sin(\theta)] \\ &= \cos(\theta) - \cos(\Delta\theta + \theta) = \cos(\theta) - \cos(\theta') \\ &= -2\sin\left(\frac{\theta+\theta'}{2}\right)\sin\left(\frac{\theta-\theta'}{2}\right) = 2\sin\left(\frac{\theta+\theta'}{2}\right)\sin\left(\frac{\theta'-\theta}{2}\right) \\ &= 2\sin(\bar{\theta})\sin\left(\frac{\Delta\theta}{2}\right),\end{aligned}$$

and

$$\begin{aligned}
 & -\left(c'_h/c_h\right)\sin(\Delta\theta)\cos(\theta)+\left[1-\left(c'_h/c_h\right)\cos(\Delta\theta)\right]\sin(\theta) \\
 & =\sin(\theta)-\left(c'_h/c_h\right)\left[\sin(\Delta\theta)\cos(\theta)+\cos(\Delta\theta)\sin(\theta)\right] \\
 & =\sin(\theta)-\left(c'_h/c_h\right)\sin(\Delta\theta+\theta)=\sin(\theta)-\left(c'_h/c_h\right)\sin(\theta') \\
 & =\sin\left(\bar{\theta}-\frac{\Delta\theta}{2}\right)-\left(c'_h/c_h\right)\sin\left(\bar{\theta}+\frac{\Delta\theta}{2}\right) \\
 & =\sin(\bar{\theta})\cos\left(\frac{\Delta\theta}{2}\right)-\cos(\bar{\theta})\sin\left(\frac{\Delta\theta}{2}\right) \\
 & -\left(c'_h/c_h\right)\left[\sin(\bar{\theta})\cos\left(\frac{\Delta\theta}{2}\right)+\cos(\bar{\theta})\sin\left(\frac{\Delta\theta}{2}\right)\right] \\
 & =\left(1-c'_h/c_h\right)\sin(\bar{\theta})\cos\left(\frac{\Delta\theta}{2}\right)-\left(1+c'_h/c_h\right)\cos(\bar{\theta})\sin\left(\frac{\Delta\theta}{2}\right),
 \end{aligned}$$

where we have defined the average chiral angle as $\bar{\theta} \equiv \frac{\theta+\theta'}{2}$ and used the relations $\theta' = \bar{\theta} + \frac{\Delta\theta}{2}$ and $\theta = \bar{\theta} - \frac{\Delta\theta}{2}$.

With this we have:

$$\begin{aligned}
 & L_1^M \\
 & =\frac{\sqrt{3}d}{\left(1+c'_h/c_h\right)\left[1-\cos(\Delta\theta)\right]}\left(\begin{array}{c} 2\sin(\bar{\theta})\sin\left(\frac{\Delta\theta}{2}\right) \\ \left(1-c'_h/c_h\right)\sin(\bar{\theta})\cos\left(\frac{\Delta\theta}{2}\right)-\left(1+c'_h/c_h\right)\cos(\bar{\theta})\sin\left(\frac{\Delta\theta}{2}\right) \end{array}\right)
 \end{aligned}$$

Since $1-\cos(\Delta\theta)=2\sin^2\left(\frac{\Delta\theta}{2}\right)$ we have:

$$\begin{aligned}
 & L_1^M \\
 & =\frac{\sqrt{3}d}{2\left(1+c'_h/c_h\right)\sin^2\left(\frac{\Delta\theta}{2}\right)}\left(\begin{array}{c} 2\sin(\bar{\theta})\sin\left(\frac{\Delta\theta}{2}\right) \\ \left(1-c'_h/c_h\right)\sin(\bar{\theta})\cos\left(\frac{\Delta\theta}{2}\right)-\left(1+c'_h/c_h\right)\cos(\bar{\theta})\sin\left(\frac{\Delta\theta}{2}\right) \end{array}\right) \\
 & =\frac{\sqrt{3}d}{2\left(1+c'_h/c_h\right)\sin\left(\frac{\Delta\theta}{2}\right)}\left(\begin{array}{c} 2\sin(\bar{\theta}) \\ \left(1-c'_h/c_h\right)\sin(\bar{\theta})\cot\left(\frac{\Delta\theta}{2}\right)-\left(1+c'_h/c_h\right)\cos(\bar{\theta}) \end{array}\right) \\
 & =\frac{\sqrt{3}d\sin(\bar{\theta})}{2\left(1+c'_h/c_h\right)\sin\left(\frac{\Delta\theta}{2}\right)}\left(\begin{array}{c} 2 \\ \left(1-c'_h/c_h\right)\cot\left(\frac{\Delta\theta}{2}\right)-\left(1+c'_h/c_h\right)\cot(\bar{\theta}) \end{array}\right) \\
 & =\frac{\sqrt{3}d\sin(\bar{\theta})}{2\left(1+c'_h/c_h\right)\sin\left(\frac{\Delta\theta}{2}\right)}\left\{2\hat{\mathbf{x}}+\left[\left(1-c'_h/c_h\right)\cot\left(\frac{\Delta\theta}{2}\right)-\left(1+c'_h/c_h\right)\cot(\bar{\theta})\right]\hat{\mathbf{y}}\right\}
 \end{aligned}$$

Namely,

$$\boxed{L_1^M = \frac{\sqrt{3}d\sin(\bar{\theta})}{2\left(1+c'_h/c_h\right)\sin\left(\frac{\Delta\theta}{2}\right)}\left\{2\hat{\mathbf{x}}+\left[\left(1-c'_h/c_h\right)\cot\left(\frac{\Delta\theta}{2}\right)-\left(1+c'_h/c_h\right)\cot(\bar{\theta})\right]\hat{\mathbf{y}}\right\}.}$$

Since the (\tilde{x}, \tilde{y}) is orthogonal the size of L_1^M is given by:

$$L_1^M = \frac{\sqrt{3}d\sin(\bar{\theta})}{2(1 + c'_h/c_h)|\sin(\frac{\Delta\theta}{2})|} \sqrt{4 + \left[(1 - c'_h/c_h) \cot\left(\frac{\Delta\theta}{2}\right) - (1 + c'_h/c_h) \cot(\bar{\theta}) \right]^2}$$

The angle that L_1^M forms with the main axis of the DWNT (\hat{y}') is given by:

$$\cos(\alpha) = \frac{L_1^M \cdot \hat{y}}{L_1^M} = \text{sgn} \left[\sin\left(\frac{\Delta\theta}{2}\right) \right] \frac{(1 - c'_h/c_h) \cot\left(\frac{\Delta\theta}{2}\right) - (1 + c'_h/c_h) \cot(\bar{\theta})}{\sqrt{4 + \left[(1 - c'_h/c_h) \cot\left(\frac{\Delta\theta}{2}\right) - (1 + c'_h/c_h) \cot(\bar{\theta}) \right]^2}}$$

The second Moiré supercell lattice vector L_2^M

The second Moiré supercell lattice vector is given by:

$$\begin{aligned} L_2^M &= (I - \mathcal{R}^{-1}\mathcal{M}^{-1})^{-1}\tilde{\mathbf{a}}_2 \\ &= \frac{\sqrt{3}d}{(1 + c'_h/c_h)[1 - \cos(\Delta\theta)]} \begin{pmatrix} 1 - \cos(\Delta\theta) & \sin(\Delta\theta) \\ -(c'_h/c_h)\sin(\Delta\theta) & 1 - (c'_h/c_h)\cos(\Delta\theta) \end{pmatrix} \begin{pmatrix} \cos\left(\theta - \frac{\pi}{3}\right) \\ \sin\left(\theta - \frac{\pi}{3}\right) \end{pmatrix} \\ &= \frac{\sqrt{3}d}{(1 + c'_h/c_h)[1 - \cos(\Delta\theta)]} \begin{pmatrix} [1 - \cos(\Delta\theta)] \cos\left(\theta - \frac{\pi}{3}\right) + \sin(\Delta\theta) \sin\left(\theta - \frac{\pi}{3}\right) \\ -(c'_h/c_h)\sin(\Delta\theta) \cos\left(\theta - \frac{\pi}{3}\right) + [1 - (c'_h/c_h)\cos(\Delta\theta)] \sin\left(\theta - \frac{\pi}{3}\right) \end{pmatrix} \end{aligned}$$

Looking separately on each vector element we get:

$$\begin{aligned} & [1 - \cos(\Delta\theta)] \cos\left(\theta - \frac{\pi}{3}\right) + \sin(\Delta\theta) \sin\left(\theta - \frac{\pi}{3}\right) \\ &= \cos\left(\theta - \frac{\pi}{3}\right) - \left[\cos(\Delta\theta) \cos\left(\theta - \frac{\pi}{3}\right) - \sin(\Delta\theta) \sin\left(\theta - \frac{\pi}{3}\right) \right] \\ &= \cos\left(\theta - \frac{\pi}{3}\right) - \cos\left(\Delta\theta + \theta - \frac{\pi}{3}\right) = \cos\left(\theta - \frac{\pi}{3}\right) - \cos\left(\theta' - \frac{\pi}{3}\right) \\ &= -2 \sin\left(\frac{\theta - \frac{\pi}{3} + \theta' - \frac{\pi}{3}}{2}\right) \sin\left(\frac{\theta - \frac{\pi}{3} - \theta' + \frac{\pi}{3}}{2}\right) = 2 \sin\left(\frac{\theta + \theta'}{2} - \frac{\pi}{3}\right) \sin\left(\frac{\theta' - \theta}{2}\right) \\ &= 2 \sin\left(\bar{\theta} - \frac{\pi}{3}\right) \sin\left(\frac{\Delta\theta}{2}\right) \end{aligned}$$

and

$$\begin{aligned}
 & - (c'_h/c_h) \sin(\Delta\theta) \cos\left(\theta - \frac{\pi}{3}\right) + [1 - (c'_h/c_h) \cos(\Delta\theta)] \sin\left(\theta - \frac{\pi}{3}\right) \\
 & = \sin\left(\theta - \frac{\pi}{3}\right) \\
 & - (c'_h/c_h) \left[\sin(\Delta\theta) \cos\left(\theta - \frac{\pi}{3}\right) + \cos(\Delta\theta) \sin\left(\theta - \frac{\pi}{3}\right) \right] \\
 & = \sin\left(\theta - \frac{\pi}{3}\right) - (c'_h/c_h) \sin\left(\Delta\theta + \theta - \frac{\pi}{3}\right) \\
 & = \sin\left(\theta - \frac{\pi}{3}\right) - (c'_h/c_h) \sin\left(\theta' - \frac{\pi}{3}\right) \\
 & = \sin\left(\bar{\theta} - \frac{\Delta\theta}{2} - \frac{\pi}{3}\right) - (c'_h/c_h) \sin\left(\bar{\theta} + \frac{\Delta\theta}{2} - \frac{\pi}{3}\right) \\
 & = \sin\left[\left(\bar{\theta} - \frac{\pi}{3}\right) - \frac{\Delta\theta}{2}\right] - (c'_h/c_h) \sin\left[\left(\bar{\theta} - \frac{\pi}{3}\right) + \frac{\Delta\theta}{2}\right] \\
 & = \sin\left(\bar{\theta} - \frac{\pi}{3}\right) \cos\left(\frac{\Delta\theta}{2}\right) - \cos\left(\bar{\theta} - \frac{\pi}{3}\right) \sin\left(\frac{\Delta\theta}{2}\right) \\
 & - (c'_h/c_h) \sin\left(\bar{\theta} - \frac{\pi}{3}\right) \cos\left(\frac{\Delta\theta}{2}\right) - (c'_h/c_h) \cos\left(\bar{\theta} - \frac{\pi}{3}\right) \sin\left(\frac{\Delta\theta}{2}\right) \\
 & = (1 - c'_h/c_h) \sin\left(\bar{\theta} - \frac{\pi}{3}\right) \cos\left(\frac{\Delta\theta}{2}\right) \\
 & - (1 + c'_h/c_h) \cos\left(\bar{\theta} - \frac{\pi}{3}\right) \sin\left(\frac{\Delta\theta}{2}\right)
 \end{aligned}$$

Giving:

$$L_2^M = \frac{\sqrt{3}d}{(1 + c'_h/c_h)[1 - \cos(\Delta\theta)]} \left(\begin{array}{c} 2 \sin\left(\bar{\theta} - \frac{\pi}{3}\right) \sin\left(\frac{\Delta\theta}{2}\right) \\ (1 - c'_h/c_h) \sin\left(\bar{\theta} - \frac{\pi}{3}\right) \cos\left(\frac{\Delta\theta}{2}\right) - (1 + c'_h/c_h) \cos\left(\bar{\theta} - \frac{\pi}{3}\right) \sin\left(\frac{\Delta\theta}{2}\right) \end{array} \right)$$

Since $1 - \cos(\Delta\theta) = 2\sin^2\left(\frac{\Delta\theta}{2}\right)$ we have:

$$\begin{aligned}
 L_2^M & = \frac{\sqrt{3}d}{2(1 + c'_h/c_h)\sin^2\left(\frac{\Delta\theta}{2}\right)} \left(\begin{array}{c} 2 \sin\left(\bar{\theta} - \frac{\pi}{3}\right) \sin\left(\frac{\Delta\theta}{2}\right) \\ (1 - c'_h/c_h) \sin\left(\bar{\theta} - \frac{\pi}{3}\right) \cos\left(\frac{\Delta\theta}{2}\right) - (1 + c'_h/c_h) \cos\left(\bar{\theta} - \frac{\pi}{3}\right) \sin\left(\frac{\Delta\theta}{2}\right) \end{array} \right) \\
 & = \frac{\sqrt{3}d}{2(1 + c'_h/c_h)\sin\left(\frac{\Delta\theta}{2}\right)} \left(\begin{array}{c} 2 \sin\left(\bar{\theta} - \frac{\pi}{3}\right) \\ (1 - c'_h/c_h) \sin\left(\bar{\theta} - \frac{\pi}{3}\right) \cot\left(\frac{\Delta\theta}{2}\right) - (1 + c'_h/c_h) \cos\left(\bar{\theta} - \frac{\pi}{3}\right) \end{array} \right) \\
 & = \frac{\sqrt{3}d \sin\left(\bar{\theta} - \frac{\pi}{3}\right)}{2(1 + c'_h/c_h)\sin\left(\frac{\Delta\theta}{2}\right)} \left(\begin{array}{c} 2 \\ (1 - c'_h/c_h) \cot\left(\frac{\Delta\theta}{2}\right) - (1 + c'_h/c_h) \cot\left(\bar{\theta} - \frac{\pi}{3}\right) \end{array} \right) \\
 & = \frac{\sqrt{3}d \sin\left(\bar{\theta} - \frac{\pi}{3}\right)}{2(1 + c'_h/c_h)\sin\left(\frac{\Delta\theta}{2}\right)} \left\{ 2\hat{\mathbf{x}} + \left[(1 - c'_h/c_h) \cot\left(\frac{\Delta\theta}{2}\right) - (1 + c'_h/c_h) \cot\left(\bar{\theta} - \frac{\pi}{3}\right) \right] \hat{\mathbf{y}} \right\}
 \end{aligned}$$

Namely,

$$\mathbf{L}_2^M = \frac{\sqrt{3}d \sin(\bar{\theta} - \frac{\pi}{3})}{2(1 + c'_h/c_h) \sin(\frac{\Delta\theta}{2})} \left\{ 2\hat{\mathbf{x}} + \left[(1 - c'_h/c_h) \cot(\frac{\Delta\theta}{2}) - (1 + c'_h/c_h) \cot(\bar{\theta} - \frac{\pi}{3}) \right] \hat{\mathbf{y}} \right\}.$$

Since the $(\hat{\mathbf{x}}, \hat{\mathbf{y}})$ is orthogonal the size of \mathbf{L}_2^M is given by:

$$L_2^M = -\frac{\sqrt{3}d \sin(\bar{\theta} - \frac{\pi}{3})}{2(1 + c'_h/c_h) |\sin(\frac{\Delta\theta}{2})|} \sqrt{4 + \left[(1 - c'_h/c_h) \cot(\frac{\Delta\theta}{2}) - (1 + c'_h/c_h) \cot(\bar{\theta} - \frac{\pi}{3}) \right]^2}$$

The angle that \mathbf{L}_2^M forms with the main axis of the DWNT ($\hat{\mathbf{y}}'$) is given by:

$$\cos(\beta) = \frac{\mathbf{L}_2^M \cdot \hat{\mathbf{y}}}{L_1^M} = -\text{sgn} \left[\sin\left(\frac{\Delta\theta}{2}\right) \right] \frac{(1 - c'_h/c_h) \cot(\frac{\Delta\theta}{2}) - (1 + c'_h/c_h) \cot(\bar{\theta} - \frac{\pi}{3})}{\sqrt{4 + \left[(1 - c'_h/c_h) \cot(\frac{\Delta\theta}{2}) - (1 + c'_h/c_h) \cot(\bar{\theta} - \frac{\pi}{3}) \right]^2}}$$

Achiral ACDWNTs

For achiral ACDWNTs we have $\bar{\theta} = \frac{\pi}{6}$ and $\Delta\theta = 0$. Taking the limit $\Delta\theta \rightarrow 0$ for the length of the Moiré supercell lattice vectors gives:

$$\begin{aligned} L_1^M &= \frac{\sqrt{3}d \sin(\bar{\theta})}{2(1 + c'_h/c_h) |\sin(\frac{\Delta\theta}{2})|} \sqrt{4 + \left[(1 - c'_h/c_h) \cot(\frac{\Delta\theta}{2}) - (1 + c'_h/c_h) \cot(\bar{\theta}) \right]^2} \\ &\xrightarrow{\bar{\theta}=\frac{\pi}{6}, \Delta\theta \rightarrow 0} \frac{0.5\sqrt{3}d}{2(1 + c'_h/c_h) |\sin(\frac{\Delta\theta}{2})|} \sqrt{4 + \left[(1 - c'_h/c_h) \cot(\frac{\Delta\theta}{2}) - (1 + c'_h/c_h) \sqrt{3} \right]^2} \xrightarrow{\Delta\theta \rightarrow 0} \frac{\sqrt{3}d |1 - c'_h/c_h| |\cot(\frac{\Delta\theta}{2})|}{4(1 + c'_h/c_h) |\sin(\frac{\Delta\theta}{2})|} \\ &= \frac{\sqrt{3}d |1 - c'_h/c_h| |\cos(\frac{\Delta\theta}{2})|}{4(1 + c'_h/c_h) \sin^2(\frac{\Delta\theta}{2})} \xrightarrow{\Delta\theta \rightarrow 0} \frac{\sqrt{3}d |1 - c'_h/c_h|}{4(1 + c'_h/c_h) \sin^2(\frac{\Delta\theta}{2})} \xrightarrow{\Delta\theta \rightarrow 0} \infty. \end{aligned}$$

$$\begin{aligned} L_2^M &= -\frac{\sqrt{3}d \sin(\bar{\theta} - \frac{\pi}{3})}{2(1 + c'_h/c_h) |\sin(\frac{\Delta\theta}{2})|} \sqrt{4 + \left[(1 - c'_h/c_h) \cot(\frac{\Delta\theta}{2}) - (1 + c'_h/c_h) \cot(\bar{\theta} - \frac{\pi}{3}) \right]^2} \\ &\xrightarrow{\bar{\theta}=\frac{\pi}{6}, \Delta\theta \rightarrow 0} \frac{0.5\sqrt{3}d}{2(1 + c'_h/c_h) |\sin(\frac{\Delta\theta}{2})|} \sqrt{4 + \left[(1 - c'_h/c_h) \cot(\frac{\Delta\theta}{2}) + (1 + c'_h/c_h) \sqrt{3} \right]^2} \xrightarrow{\Delta\theta \rightarrow 0} \end{aligned}$$

$$\frac{\sqrt{3}d|1 - c'_h/c_h| |\cot(\frac{\Delta\theta}{2})|}{4(1 + c'_h/c_h) |\sin(\frac{\Delta\theta}{2})|} = \frac{\sqrt{3}d|1 - c'_h/c_h| |\cos(\frac{\Delta\theta}{2})|}{4(1 + c'_h/c_h) \sin^2(\frac{\Delta\theta}{2})}$$

$$= \xrightarrow{\Delta\theta \rightarrow 0} \frac{\sqrt{3}d|1 - c'_h/c_h|}{4(1 + c'_h/c_h)} \frac{1}{\sin^2(\frac{\Delta\theta}{2})} \xrightarrow{\Delta\theta \rightarrow 0} \infty$$

Hence, the Moiré supercell lattice vectors become infinite in length for the case of achiral ACDWNTs.

The alignment of the Moiré supercell lattice with respect to the axis of the DWNT can be obtained from the angles between the supercell lattice vectors and the translational vector of the tube. For L_1^M we have:

$$\cos(\alpha) = \text{sgn} \left[\sin \left(\frac{\Delta\theta}{2} \right) \right] \frac{(1 - c'_h/c_h) \cot(\frac{\Delta\theta}{2}) - (1 + c'_h/c_h) \cot(\bar{\theta})}{\sqrt{4 + [(1 - c'_h/c_h) \cot(\frac{\Delta\theta}{2}) - (1 + c'_h/c_h) \cot(\bar{\theta})]^2}}$$

$$\xrightarrow{\bar{\theta} = \frac{\pi}{6}, \Delta\theta \rightarrow 0} \text{sgn} \left[\sin \left(\frac{\Delta\theta}{2} \right) \right] \frac{[(1 - c'_h/c_h) \cot(\frac{\Delta\theta}{2}) - (1 + c'_h/c_h)\sqrt{3}]}{\sqrt{4 + [(1 - c'_h/c_h) \cot(\frac{\Delta\theta}{2}) - (1 + c'_h/c_h)\sqrt{3}]^2}}$$

$$\xrightarrow{\Delta\theta \rightarrow 0} \frac{(1 - c'_h/c_h) \cot(\frac{\Delta\theta}{2})}{|(1 - c'_h/c_h) \cot(\frac{\Delta\theta}{2})|} = \text{sgn} \left[(1 - c'_h/c_h) \cot \left(\frac{\Delta\theta}{2} \right) \right] \xrightarrow{\Delta\theta \rightarrow 0} -1.$$

Hence, for ACDWNTs $\alpha = 180^\circ$ such that L_1^M is antiparallel with the axis of the tube.

For L_2^M we have:

$$\cos(\beta) = -\text{sgn} \left[\sin \left(\frac{\Delta\theta}{2} \right) \right] \frac{(1 - c'_h/c_h) \cot(\frac{\Delta\theta}{2}) - (1 + c'_h/c_h) \cot(\bar{\theta} - \frac{\pi}{3})}{\sqrt{4 + [(1 - c'_h/c_h) \cot(\frac{\Delta\theta}{2}) - (1 + c'_h/c_h) \cot(\bar{\theta} - \frac{\pi}{3})]^2}}$$

$$\xrightarrow{\bar{\theta} = \frac{\pi}{6}, \Delta\theta \rightarrow 0} - \frac{(1 - c'_h/c_h) \cot(\frac{\Delta\theta}{2}) + (1 + c'_h/c_h)\sqrt{3}}{\sqrt{4 + [(1 - c'_h/c_h) \cot(\frac{\Delta\theta}{2}) + (1 + c'_h/c_h)\sqrt{3}]^2}}$$

$$\xrightarrow{\Delta\theta \rightarrow 0} - \frac{(1 - c'_h/c_h) \cot(\frac{\Delta\theta}{2})}{|(1 - c'_h/c_h) \cot(\frac{\Delta\theta}{2})|} = -\text{sgn} \left[(1 - c'_h/c_h) \cot \left(\frac{\Delta\theta}{2} \right) \right] \xrightarrow{\Delta\theta \rightarrow 0} 1$$

Hence, for ACDWNTs $\beta = 0^\circ$ such that L_2^M is parallel with the axis of the tube.

We therefore see that for achiral ACDWNTs the Moiré unit cell becomes infinitely long and infinitesimally thin and its vectors are parallel to the main axis of the tube thus forming continuous axial registry patterns.

Achiral ZZDWNTs

For achiral ZZDWNTs we have $\bar{\theta} = 0$ and $\Delta\theta = 0$. Taking the limit $\Delta\theta \rightarrow 0$ for the length of the Moiré supercell lattice vectors gives:

$$L_1^M = \frac{\sqrt{3}d\sin(\bar{\theta})}{2(1 + c'_h/c_h)|\sin(\frac{\Delta\theta}{2})|} \sqrt{4 + \left[(1 - c'_h/c_h) \cot\left(\frac{\Delta\theta}{2}\right) - (1 + c'_h/c_h) \cot(\bar{\theta}) \right]^2}$$

$$\xrightarrow{\bar{\theta} \rightarrow 0, \Delta\theta \rightarrow 0} \frac{\sqrt{3}d}{2(1 + c'_h/c_h)} \left| (1 - c'_h/c_h) \cot\left(\frac{\Delta\theta}{2}\right) - (1 + c'_h/c_h) \cot(\bar{\theta}) \right| \xrightarrow{\Delta\theta \rightarrow 0} \infty.$$

$$L_2^M = \frac{3d}{4(1 + c'_h/c_h)|\sin(\frac{\Delta\theta}{2})|} \sqrt{4 + \left[(1 - c'_h/c_h) \cot\left(\frac{\Delta\theta}{2}\right) + (1 + c'_h/c_h) \sqrt{3}/3 \right]^2}$$

$$\xrightarrow{\Delta\theta \rightarrow 0} \frac{3d}{4(1 + c'_h/c_h)\sin(\frac{\Delta\theta}{2})} \left| (1 - c'_h/c_h) \cot\left(\frac{\Delta\theta}{2}\right) \right|$$

$$= \frac{3d|(1 - c'_h/c_h)| \cot(\frac{\Delta\theta}{2})}{4(1 + c'_h/c_h) \sin(\frac{\Delta\theta}{2})}$$

$$= \frac{3d|(1 - c'_h/c_h)| \cos(\frac{\Delta\theta}{2})}{4(1 + c'_h/c_h) \sin^2(\frac{\Delta\theta}{2})} \xrightarrow{\Delta\theta \rightarrow 0} \frac{3d|(1 - c'_h/c_h)|}{4(1 + c'_h/c_h)} \frac{1}{\sin^2(\frac{\Delta\theta}{2})} \xrightarrow{\Delta\theta \rightarrow 0} \infty$$

Hence, the Moiré supercell lattice vectors become infinite in length also for the case of achiral ZZDWNTs.

The alignment of the Moiré supercell lattice with respect to the axis of the DWNT can be obtained from the angles between the supercell lattice vectors and the translational vector of the tube. For L_1^M we have:

$$\cos(\alpha)$$

$$= \text{sgn} \left[\sin\left(\frac{\Delta\theta}{2}\right) \right] \frac{(1 - c'_h/c_h) \cot(\frac{\Delta\theta}{2}) - (1 + c'_h/c_h) \cot(\bar{\theta})}{\sqrt{4 + \left[(1 - c'_h/c_h) \cot(\frac{\Delta\theta}{2}) - (1 + c'_h/c_h) \cot(\bar{\theta}) \right]^2}} \xrightarrow{\bar{\theta} \rightarrow 0, \Delta\theta \rightarrow 0}$$

$$\frac{(1 - c'_h/c_h) \cot(\frac{\Delta\theta}{2}) - (1 + c'_h/c_h) \cot(\bar{\theta})}{|(1 - c'_h/c_h) \cot(\frac{\Delta\theta}{2}) - (1 + c'_h/c_h) \cot(\bar{\theta})|}$$

$$= \text{sgn} \left[(1 - c'_h/c_h) \cot\left(\frac{\Delta\theta}{2}\right) - (1 + c'_h/c_h) \cot(\bar{\theta}) \right] \xrightarrow{\bar{\theta} \rightarrow 0, \Delta\theta \rightarrow 0} -1.$$

Hence, for ZZDWNTs as well $\alpha = 180^\circ$ such that L_1^M is antiparallel with the axis of the tube.

For L_2^M we have:

$$\cos(\beta) = -\text{sgn} \left[\sin\left(\frac{\Delta\theta}{2}\right) \right] \frac{(1 - c'_h/c_h) \cot(\frac{\Delta\theta}{2}) - (1 + c'_h/c_h) \cot(\bar{\theta} - \frac{\pi}{3})}{\sqrt{4 + [(1 - c'_h/c_h) \cot(\frac{\Delta\theta}{2}) - (1 + c'_h/c_h) \cot(\bar{\theta} - \frac{\pi}{3})]^2}}$$

$$\xrightarrow{\bar{\theta} \rightarrow 0, \Delta\theta \rightarrow 0} - \frac{(1 - c'_h/c_h) \cot(\frac{\Delta\theta}{2}) + (1 + c'_h/c_h) \sqrt{3}/3}{\sqrt{4 + [(1 - c'_h/c_h) \cot(\frac{\Delta\theta}{2}) - (1 + c'_h/c_h) \sqrt{3}/3]^2}} \xrightarrow{\Delta\theta \rightarrow 0}$$

$$- \frac{(1 - c'_h/c_h) \cot(\frac{\Delta\theta}{2})}{|(1 - c'_h/c_h) \cot(\frac{\Delta\theta}{2})|} = -\text{sgn} \left[(1 - c'_h/c_h) \cot\left(\frac{\Delta\theta}{2}\right) \right] \xrightarrow{\Delta\theta \rightarrow 0} 1$$

Hence, for ZZDWNTs as well $\beta = 0^\circ$ such that L_2^M is parallel with the axis of the tube.

We therefore see that like achiral ACDWNTs for ZZDWNTs the Moiré unit cell becomes infinitely long and infinitesimally thin and its vectors are parallel to the main axis of the tube thus forming continuous axial registry patterns.

Monochiral DWNTs

For monochiral DWNTs we have $0 < \bar{\theta} < \frac{\pi}{6}$ and $\Delta\theta = 0$. Taking the limit $\Delta\theta \rightarrow 0$ for the length of the Moiré supercell lattice vectors gives:

$$L_1^M$$

$$= \frac{\sqrt{3}d\sin(\bar{\theta})}{2(1 + c'_h/c_h)|\sin(\frac{\Delta\theta}{2})|} \sqrt{4 + [(1 - c'_h/c_h) \cot(\frac{\Delta\theta}{2}) - (1 + c'_h/c_h) \cot(\bar{\theta})]^2} \xrightarrow{0 < \bar{\theta} < \frac{\pi}{6}, \Delta\theta \rightarrow 0}$$

$$\begin{aligned} & \frac{\sqrt{3}d|(1 - c'_h/c_h)|\sin(\bar{\theta})\cot(\frac{\Delta\theta}{2})}{2(1 + c'_h/c_h)\sin(\frac{\Delta\theta}{2})} \\ &= \frac{\sqrt{3}d|(1 - c'_h/c_h)|\sin(\bar{\theta})\cos(\frac{\Delta\theta}{2})}{2(1 + c'_h/c_h)\sin^2(\frac{\Delta\theta}{2})} \xrightarrow{0 < \bar{\theta} < \frac{\pi}{6}, \Delta\theta \rightarrow 0} \frac{\sqrt{3}d|(1 - c'_h/c_h)|\sin(\bar{\theta})}{2(1 + c'_h/c_h)} \frac{1}{\sin^2(\frac{\Delta\theta}{2})} \xrightarrow{0 < \bar{\theta} < \frac{\pi}{6}, \Delta\theta \rightarrow 0} \infty \end{aligned}$$

and

$$\begin{aligned} & L_2^M \\ &= -\frac{\sqrt{3}d\sin(\bar{\theta} - \frac{\pi}{3})}{2(1 + c'_h/c_h)|\sin(\frac{\Delta\theta}{2})|} \sqrt{4 + \left[(1 - c'_h/c_h)\cot(\frac{\Delta\theta}{2}) - (1 + c'_h/c_h)\cot(\bar{\theta} - \frac{\pi}{3}) \right]^2} \xrightarrow{0 < \bar{\theta} < \frac{\pi}{6}, \Delta\theta \rightarrow 0} \infty \\ &= -\frac{\sqrt{3}d\sin(\bar{\theta} - \frac{\pi}{3})}{2(1 + c'_h/c_h)\sin(\frac{\Delta\theta}{2})} \left| (1 - c'_h/c_h)\cot(\frac{\Delta\theta}{2}) \right| \\ &= -\frac{\sqrt{3}d\sin(\bar{\theta} - \frac{\pi}{3})|(1 - c'_h/c_h)|\cot(\frac{\Delta\theta}{2})}{2(1 + c'_h/c_h)\sin(\frac{\Delta\theta}{2})} \\ &= -\frac{\sqrt{3}d\sin(\bar{\theta} - \frac{\pi}{3})|(1 - c'_h/c_h)|\cos(\frac{\Delta\theta}{2})}{2(1 + c'_h/c_h)\sin^2(\frac{\Delta\theta}{2})} \xrightarrow{0 < \bar{\theta} < \frac{\pi}{6}, \Delta\theta \rightarrow 0} \infty \\ &= -\frac{\sqrt{3}d\sin(\bar{\theta} - \frac{\pi}{3})|(1 - c'_h/c_h)|}{2(1 + c'_h/c_h)\sin^2(\frac{\Delta\theta}{2})} \xrightarrow{0 < \bar{\theta} < \frac{\pi}{6}, \Delta\theta \rightarrow 0} \infty. \end{aligned}$$

Hence, the Moiré supercell lattice vectors become infinite in length also for the case of monochiral DWNTs.

The alignment of the Moiré supercell lattice with respect to the axis of the DWNT can be obtained from the angles between the supercell lattice vectors and the translational vector of the tube. For L_1^M we have:

$$\begin{aligned} & \cos(\alpha) \\ &= \text{sgn} \left[\sin\left(\frac{\Delta\theta}{2}\right) \right] \frac{(1 - c'_h/c_h)\cot(\frac{\Delta\theta}{2}) - (1 + c'_h/c_h)\cot(\bar{\theta})}{\sqrt{4 + \left[(1 - c'_h/c_h)\cot(\frac{\Delta\theta}{2}) - (1 + c'_h/c_h)\cot(\bar{\theta}) \right]^2}} \xrightarrow{0 < \bar{\theta} < \frac{\pi}{6}, \Delta\theta \rightarrow 0} \\ & \frac{(1 - c'_h/c_h)\cot(\frac{\Delta\theta}{2})}{|(1 - c'_h/c_h)\cot(\frac{\Delta\theta}{2})|} = \text{sgn} \left[(1 - c'_h/c_h)\cot\left(\frac{\Delta\theta}{2}\right) \right] = -1 \end{aligned}$$

Hence, for monochiral DWNTs as well $\alpha = 180^\circ$ such that L_1^M is antiparallel with the axis of the tube.

For L_2^M we have:

$$\begin{aligned} & \cos(\beta) \\ &= -\text{sgn} \left[\sin \left(\frac{\Delta\theta}{2} \right) \right] \frac{(1 - c'_h/c_h) \cot(\frac{\Delta\theta}{2}) - (1 + c'_h/c_h) \cot(\bar{\theta} - \frac{\pi}{3})}{\sqrt{4 + [(1 - c'_h/c_h) \cot(\frac{\Delta\theta}{2}) - (1 + c'_h/c_h) \cot(\bar{\theta} - \frac{\pi}{3})]^2}} \xrightarrow{0 < \bar{\theta} < \frac{\pi}{6}, \Delta\theta \rightarrow 0} \\ & - \frac{(1 - c'_h/c_h) \cot(\frac{\Delta\theta}{2})}{|(1 - c'_h/c_h) \cot(\frac{\Delta\theta}{2})|} = -\text{sgn} \left[(1 - c'_h/c_h) \cot \left(\frac{\Delta\theta}{2} \right) \right] = 1 \end{aligned}$$

Hence, for monochiral DWNTs as well $\beta = 0^\circ$ such that L_2^M is parallel with the axis of the tube.

We therefore see that similar to the achiral AC and ZZDWNTs, the Moiré unit cell of the monochiral DWNTs becomes infinitely long and infinitesimally thin and its vectors are parallel to the main axis of the tube thus forming continuous axial registry patterns.

References

- 1 Stuart, S. J., Tutein, A. B. & Harrison, J. A. A reactive potential for hydrocarbons with intermolecular interactions. *J. Chem. Phys.* **112**, 6472 (2000).
- 2 Kolmogorov, A. N. & Crespi, V. H. Registry-dependent interlayer potential for graphitic systems. *Phys. Rev. B* **71**, 235415 (2005).
- 3 Tersoff, J. Modeling solid-state chemistry - interatomic potentials for multicomponent systems. *Phys. Rev. B* **39**, 5566-5568 (1989).
- 4 Leven, I., Azuri, I., Kronik, L. & Hod, O. Inter-layer potential for hexagonal boron nitride. *J. Chem. Phys.* **140**, 104106 (2014).
- 5 Hod, O. The registry index: a quantitative measure of materials' interfacial commensurability. *ChemPhysChem* **14**, 2376-2391 (2013).
- 6 Marom, N. *et al.* Stacking and registry effects in layered materials: The case of hexagonal boron nitride. *Phys. Rev. Lett.* **105**, 046801 (2010).
- 7 Gao, W. & Tkatchenko, A. Sliding mechanisms in multilayered hexagonal boron nitride and graphene: the effects of directionality, thickness, and sliding constraints. *Physical review letters* **114**, 096101, doi:10.1103/PhysRevLett.114.096101 (2015).
- 8 Koshino, M., Moon, P. & Son, Y.-W. Incommensurate double-walled carbon nanotubes as one-dimensional moiré crystals. *Phys. Rev. B* **91**, 035405 (2015).
- 9 Hod, O. Quantifying the stacking registry matching in layered materials. *Isr. J. Chem.* **50**, 506-514 (2010).